doi:10.1016/j.jmb.2008.11.055 J. Mol. Biol. (2009) 386, 391–405

JMB

Available online at www.sciencedirect.com

ScienceDirect

ELSEVIER

Alternate Binding Modes for a Ubiquitin–SH3 Domain Interaction Studied by NMR Spectroscopy

Dmitry M. Korzhnev[1,2,3], Irina Bezsonova[3], Soyoung Lee[4], Tigran V. Chalikian[4] and Lewis E. Kay[1,2,3]*

[1]*Department of Molecular Genetics, University of Toronto, Toronto, Ontario, Canada M5S 1A8*

[2]*Department of Biochemistry, University of Toronto, Toronto, Ontario, Canada M5S 1A8*

[3]*Department of Chemistry, University of Toronto, Toronto, Ontario, Canada M5S 1A8*

[4]*Department of Pharmaceutical Sciences, Leslie Dan Faculty of Pharmacy, University of Toronto, Toronto, Ontario, Canada M5S 3M2*

Received 14 October 2008; received in revised form 26 November 2008; accepted 26 November 2008
Available online 6 December 2008

Edited by P. Wright

Surfaces of many binding domains are plastic, enabling them to interact with multiple targets. An understanding of how they bind and recognize their partners is therefore predicated on characterizing such dynamic interfaces. Yet, these interfaces are difficult to study by standard biophysical techniques that often 'freeze' out conformations or that produce data averaged over an ensemble of conformers. In this study, we used NMR spectroscopy to study the interaction between the C-terminal SH3 domain of CIN85 and ubiquitin that involves the 'classical' binding sites of these proteins. Notably, chemical shift titration data of one target with another and relaxation dispersion data that report on millisecond time scale exchange processes are both well fit to a simple binding model in which free protein is in equilibrium with a single bound conformation. However, dissociation constants and chemical shift differences between free and bound states measured from both classes of experiment are in disagreement. It is shown that the data can be reconciled by considering three-state binding models involving two distinct bound conformations. By combining titration and dispersion data, kinetic and thermodynamic parameters of the three-state binding reaction are obtained along with chemical shifts for each state. A picture emerges in which one bound conformer has increased entropy and enthalpy relative to the second and chemical shifts similar to that of the free state, suggesting a less packed interface. This study provides an example of the interplay between entropy and enthalpy to fine-tune molecular interactions involving the same binding surfaces.

Keywords: ubiquitin; SH3 domain; relaxation dispersion NMR; binding modes

Introduction

Protein association reactions can be characterized by a large variety of biophysical techniques.[1,2] Structures produced by such methods as X-ray diffraction and NMR spectroscopy provide detailed atomistic descriptions of the end points of the binding reaction (i.e., free and bound forms of the molecular players)[3] but do not report directly on the kinetics or thermodynamics of the binding process. Calorimetric approaches are extremely powerful for obtaining detailed thermodynamic parameters that describe binding,[4] but site-specific information about the interactions that contribute to the energetics are difficult to infer from the thermodynamic techniques alone. Kinetic measurements report directly on rates of binding[5] but provide little information about the atomic-level details of the association. For reactions involving more than two states, placement of each of the states along the reaction pathway is often difficult.

In principle, NMR spectroscopy can circumvent many of the limitations associated with other techniques (i) because it is a high-resolution method that provides detailed site-specific information and (ii) because experiments have been developed for probing the kinetics and thermodynamics of exchange processes over a range of time scales that extend from the second to the microsecond.[6–10] Not surprisingly, therefore, NMR has emerged as a very

*Corresponding author. Department of Molecular Genetics, University of Toronto, Toronto, Ontario, Canada M5S 1A8. E-mail address: kay@pound.med.utoronto.ca.

Abbreviations used: SH3-C, C-terminal SH3 domain; ITC, isothermal titration calorimetry; CPMG, Carr–Purcell–Meiboom–Gill.

useful technique for studies on ligand-binding reactions.[11–15] Among the most established of experiments are those that record chemical shift changes of one molecular partner as a function of increasing concentrations of a second partner that can provide estimates of affinity constants. Concomitant changes in linewidths of resonances can often also be quantified to obtain the kinetics of the exchange process.[16,17] In the great majority of cases, these titrations are analyzed in terms of a simple single-step binding process involving free and bound protein states that assumes the absence of intermediates. Very often, high-quality data fits are obtained, suggesting that the simple binding model may be appropriate. However, the fact that few intermediate states have been detected may also simply reflect the fact that if formed they are present at low concentrations and hence escape detection, or that under the conditions of the titration they are in rapid exchange with either free or bound states, rendering their observation and characterization difficult. In what follows, we provide one such example.

In this work, we present a study on the binding of ubiquitin to the C-terminal SH3 domain from the adaptor protein CIN85 (SH3-C), an interaction that modulates the ubiquitination of both CIN85 and the epidermal growth factor receptor (EGFR), leading ultimately to down-regulation of EGFR activity.[18,19] This is a particularly interesting system because ubiquitin does not contain a proline-rich motif that is normally associated with binding to SH3 domains. A very recent structural model for the ubiqituin–SH3-C complex has been proposed based on solution NMR data,[20] showing that the site of interaction includes the surface of SH3-C that would normally bind proline-rich motifs as well as a hydrophobic patch on the surface of ubiquitin centered at Ile44, a region involved in the interaction of ubiquitin with most of its target proteins.[21] Chemical shift titrations involving the addition of unlabeled ubiquitin to ^{15}N-labeled SH3-C or *vice versa* could be very well fit to a simple P + L ↔ PL binding model producing dissociation constants, K_d, on the order of 200 μM. However, these values are not consistent with those obtained from additional NMR experiments that explored the kinetics of the binding reaction. Relaxation dispersion measurements that quantify exchange contributions to ^{15}N linewidths in spectra were recorded that, assuming the simple P + L ↔ PL binding model, provide exchange rates between free and bound conformers as well as chemical shift differences between the interconverting states.[7] Here, too, the data are fully consistent with a two-state model; however, K_d values calculated are an order of magnitude larger (~3–4 mM), while the shift differences do not coincide with those expected on the basis of the titration data. This finding strongly suggests that the binding mechanism is more complex than that described by the assumed model. The titration and relaxation dispersion data are, however, consistent with a model of three-state binding that involves a pair of distinct binding modes, and a combined analysis that includes titration profiles, relaxation dispersion data recorded over a range of temperatures, and isothermal titration calorimetry (ITC) measurements[4] provides the thermodynamics and kinetics of the binding reaction. Because the dispersion data are sensitive to chemical shifts of the interconverting states, structural information for both bound conformers are obtained,[22,23] and the picture that emerges from these data is consistent with expectations based on the measured thermodynamic parameters. This work thus provides a powerful demonstration of how a combination of methods, each of which is consistent with the simplest of binding models, can be used to generate a detailed picture of a more complex binding mechanism involving the formation of alternative binding modes.

Results and Discussion

Ubiquitin–SH3-C binding probed by solution NMR studies

NMR spectroscopy has long been regarded as a primary experimental technique for studies on weak protein interactions because of the exquisite sensitivity of NMR chemical shifts to small perturbations of the local electronic environment that accompany the titration of one protein with another. To avoid excessive line broadening, titration experiments are performed under conditions where the exchange between free and bound forms of the protein is fast on the NMR time scale and the data are typically well described by a simple two-state binding model, P + L ↔ PL. This is the case for the binding of ubiquitin and SH3-C at 25 °C illustrated in Fig. 1, which shows titration profiles of ^{15}N chemical shifts of ^{15}N-labeled protein P as a function of added unlabeled binding partner L. In Fig. 1a, profiles where P is ^{15}N-labeled ubiquitin and L is unlabeled SH3-C are illustrated; this order is reversed in Fig. 1b. Titration curves for 30 NH groups of ubiquitin (or 23 for SH3-C) were fit together to a model of a two-state binding process, P + L ↔ PL, yielding a dissociation constant, $K_{d,titr}$, that is a global parameter and chemical shift differences between bound and free states, $\Delta\varpi_{titr}$, that are specific for each NH moiety. $K_{d,titr}$ values of 167±22 and 215±13 μM were obtained when ^{15}N-labeled ubiquitin (Fig. 1a) and ^{15}N-labeled SH3-C (Fig. 1b) were titrated with their unlabeled partners, respectively. It is clear from Fig. 1 that high-quality fits of the data are obtained, with similar values of $K_{d,titr}$ measured from both sets of titrations. The data are thus consistent with a simple binding model, and if, in fact, multiple binding modes are present, they cannot be inferred from these experiments alone.

In the past few years, NMR relaxation dispersion methods have become a powerful tool for studies of protein interactions in cases where chemical shift differences between corresponding nuclei in the free and bound protein states are on the order of the

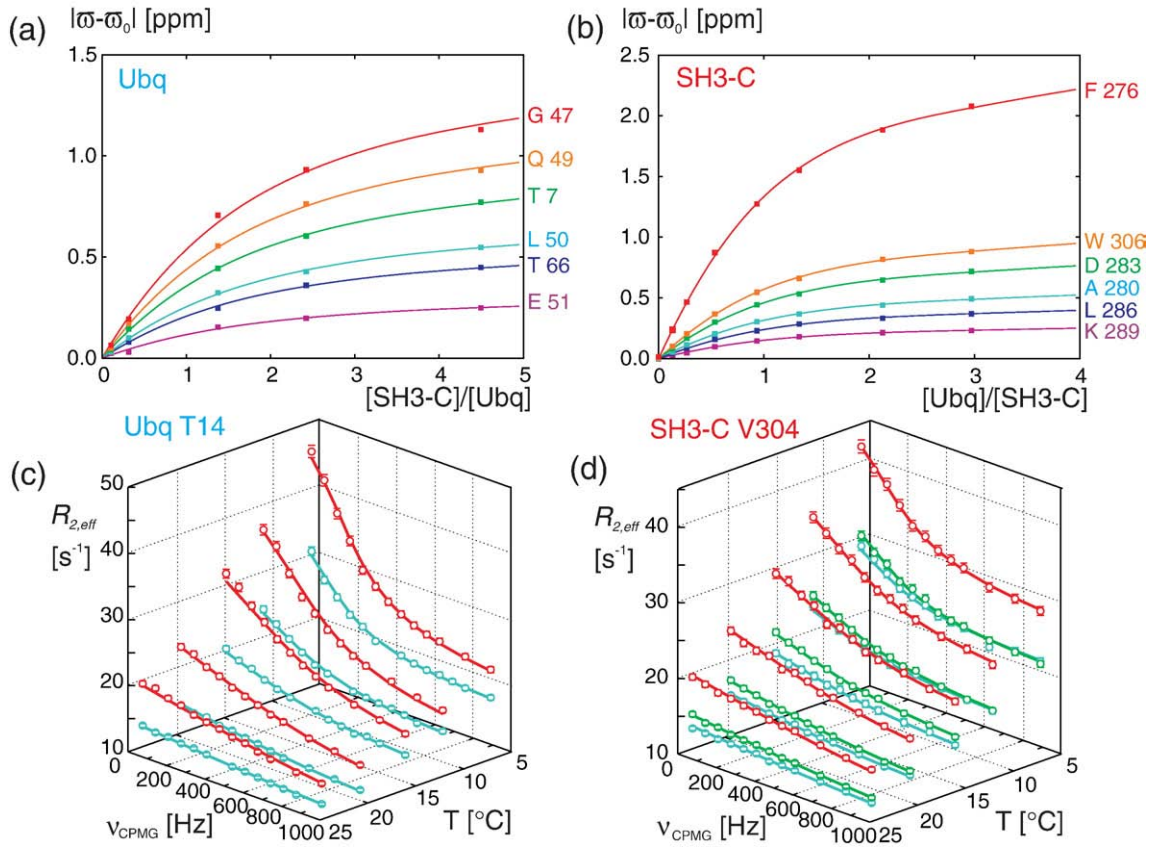

Fig. 1. Titration and relaxation dispersion data are well fit to a two-state binding model. (a and b) Typical fits of NMR titration profiles (25 °C) for select residues of ^{15}N-labeled ubiquitin titrated with unlabeled SH3-C (a) and *vice versa* (b). (c and d) Temperature-dependent ^{15}N CPMG relaxation dispersion data measured either at two or three magnetic fields (blue, 11.7 T; green, 14.1 T; red, 18.8 T) for Thr14 of ^{15}N-labeled ubiquitin (1.0 mM)/unlabeled SH3-C (0.11 mM) (c) and Val304 of ^{15}N-labeled SH3-C (1.2 mM)/unlabeled ubiquitin (0.15 mM) (d). All fits (continuous lines) are to a global two-state binding model, P + L ↔ PL.

exchange rate, corresponding to the intermediate exchange regime.[24–26] This situation leads to exchange line broadening that is undesired in titration experiments and in experiments that are used for structure determination. Contributions to linewidths of resonances from conformational exchange on the millisecond time scale can be quantified by relaxation dispersion NMR, providing detailed information on the exchange process. Here, effective transverse relaxation rates, $R_{2,\mathrm{eff}}$, that are directly related to linewidths are modulated by application of radiofrequency pulses to produce Carr–Purcell–Meiboom–Gill (CPMG) relaxation dispersion profiles[7,27,28] that plot $R_{2,\mathrm{eff}}$ as a function of a parameter that depends on the number of pulses, ν_{CPMG}. Such plots can be fit to the appropriate exchange model to extract the thermodynamics and kinetics of the reaction along with structural information in the form of chemical shifts of the interconverting conformers.[22,29]

Figure 1c highlights ^{15}N relaxation dispersion profiles measured at five temperatures and two static magnetic fields for Thr14 of an ^{15}N-labeled ubiquitin (1.0 mM) sample prepared with unlabeled SH3-C (0.11 mM). The corresponding data for Val304 of ^{15}N-labeled SH3-C (1.2 mM) with unlabeled ubiquitin (0.15 mM), recorded at three static magnetic fields, are illustrated in Fig. 1d. As expected, relatively small exchange contributions to ^{15}N transverse relaxation were observed at 25 °C, where exchange between free and bound protein states is fast on the NMR chemical shift time scale, while pronounced dispersion profiles were obtained at lower temperatures, where exchange rates slow into the intermediate regime. The data for 27 NH groups of ^{15}N-labeled ubiquitin (12 NH groups of ^{15}N-labeled SH3-C) at all temperatures and magnetic fields were fit together to the simple binding model, $P + L \underset{k_{off}}{\overset{k_{on}}{\rightleftharpoons}} PL$, assuming that (i) the temperature dependencies of the association and dissociation rate constants, k_{on} and k_{off}, respectively, obey transition-state theory[30] and that (ii) the chemical shift differences between bound and free states, $\Delta\varpi_{\mathrm{disp}}$, are independent of temperature.[22] The continuous lines correspond to the fits of the experimental data (circles), and it is clear that profiles from both ^{15}N-labeled ubiquitin and ^{15}N-labeled SH3-C are (independently) well fit by the two-state binding model, with reduced χ^2 target functions of 0.85 and 0.66, respectively.

The populations of the bound and free forms of the protein are directly accessible from fits of ^{15}N

relaxation dispersion data sets that have been recorded on samples of ubiquitin and SH3-C. The population of the bound conformer, p_B, at 25 °C is 2.8% (1.0 mM ^{15}N-labeled ubiquitin and 0.1 mM SH3-C) and 3.0% (1.2 mM ^{15}N-labeled SH3-C and 0.15 mM ubiquitin), well below the approximate value of 10% that is predicted using the $K_{d,titr}$ obtained from the titration data and the known concentrations of added proteins. The corresponding $K_{d,disp}$ values of 2.9±0.1 and 3.7± 0.3 mM (25 °C) obtained from fits of ^{15}N dispersion profiles of ubiquitin and SH3-C, respectively, are in relatively good agreement with each other but close to 1 order of magnitude higher than the $K_{d,titr}$ value of 200 μM estimated from analysis of the titrations. Notably, very different chemical shift changes upon complex formation are also obtained from the titration and relaxation dispersion methodology (Fig. 2a and b). The ^{15}N chemical shift differences between bound and free states extracted from relaxation dispersion data, $\Delta\varpi_{disp}$ (red bars in Fig. 2a and b), are systematically larger than the corresponding values of $\Delta\varpi_{titr}$ obtained from NMR titration profiles (black bars). The observed differences are far beyond the experimental uncertainties and cannot be reconciled within the framework of the two-state binding model. Thus, although both the titration and relaxation dispersion data are individually well fit assuming two-state binding and results from each type of measurement (titration or dispersion) are internally consistent in the sense that studies on ^{15}N-labeled ubiquitin–SH3-C and ^{15}N-labeled SH3-C–ubiquitin are in good agreement, the combined data strongly argue that a more complex binding process is operative.

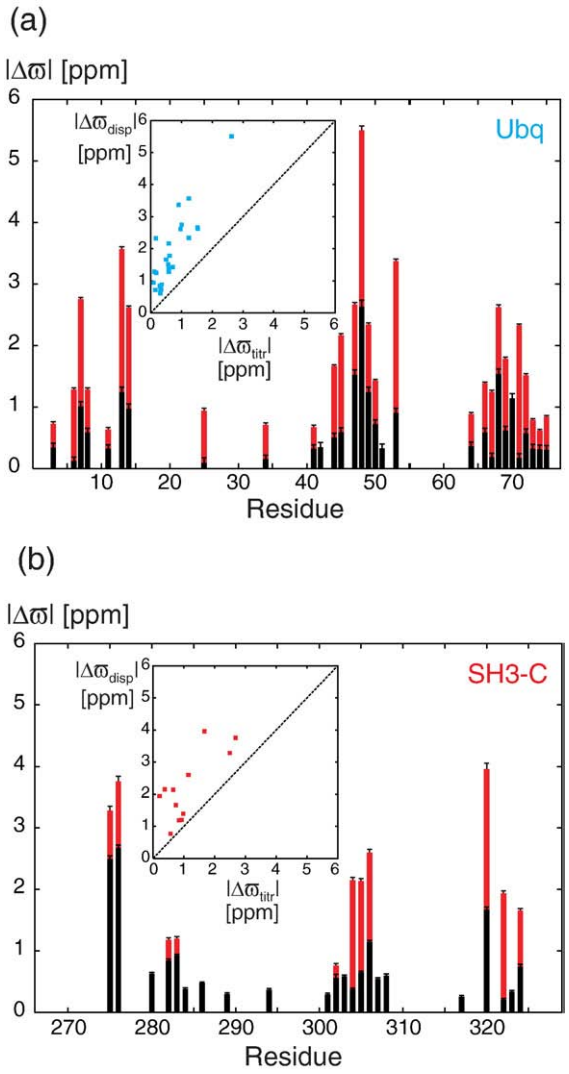

Fig. 2. Chemical shift differences from fits of titration and dispersion data to a two-state binding model were not in agreement. Backbone ^{15}N chemical shift differences between the free and bound forms of ubiquitin (a) and SH3-C (b) obtained from global fits of ^{15}N CPMG dispersion data, $|\Delta\varpi_{disp}|$ (red), and NMR titration data, $|\Delta\varpi_{titr}|$ (black), using a two-state binding model (not shown are the data for W306 $N^{\varepsilon 1}H$ of SH3-C: $|\Delta\varpi_{disp}| = 1.4 \pm 0.03$ ppm and $|\Delta\varpi_{titr}| = 0.98 \pm 0.02$ ppm). Insets to plots show correlations between $|\Delta\varpi_{disp}|$ and $|\Delta\varpi_{titr}|$.

Combining titration and relaxation dispersion data

The apparent inconsistency between the titration and relaxation dispersion data can be resolved by considering more complex binding models that involve (at least) two binding modes. In what follows, we consider the simplest of schemes involving the interconversion between P, $(PL)_1$, and $(PL)_2$, where $(PL)_1$ and $(PL)_2$ are distinct bound conformations. Such interconversions can be described by (i) $P + L \leftrightarrow (PL)_1 \leftrightarrow (PL)_2$ (consecutive binding model), (ii) $(PL)_1 \leftrightarrow P + L \leftrightarrow (PL)_2$ (parallel binding model), or (iii) a general 'triangular' model that combines the first two models (this model is more complex and is not considered here, since the first two models can fit the combined titration/dispersion data well; see below). At 25 °C, where interconversion between all states is fast, the titration data can be described by the two-state $P + L \leftrightarrow \{(PL)_1,(PL)_2\}$ binding model where the brackets indicate that $(PL)_1$ and $(PL)_2$ interconvert rapidly such that it is not possible to distinguish between them; the properties of the bound form are thus a weighted average of these two states. CPMG relaxation dispersion data recorded at lower temperatures give rise to pronounced dispersion profiles (see Fig. 1c and d), consistent with exchange between a pair of states on the millisecond time scale (intermediate exchange regime). However, the fact that excellent fits of the CPMG profiles to a two-state model are obtained implies further that two of the three states interconvert rapidly at all temperatures and cannot be separated solely on the basis of relaxation dispersion data. Note that $(PL)_1$ and $(PL)_2$ cannot interconvert rapidly at low temperatures, since then the exchange event monitored by both NMR titration and relaxation dispersion would be described by the same process, $P + L \leftrightarrow \{(PL)_1,(PL)_2\}$. Thus, K_d from titration at 25 °C would be in agreement with the corresponding value calculated at 25 °C from extracted changes in entropies/

enthalpies that are obtained from fits of the dispersion data. In addition, the chemical shift differences that are obtained from the two types of data would be identical. This is clearly not what is observed experimentally. Therefore, a three-state model emerges where at low temperatures (5–15 °C), P and one of the bound states [arbitrarily chosen to be $(PL)_1$] interconvert rapidly but other states do not, denoted in what follows by the scheme $\{P,(PL)_1\} \leftrightarrow (PL)_2$. In contrast, at higher temperatures (20–25 °C), interconversion between all states is rapid. Finally, we note in passing that flat dispersion profiles were obtained for both isolated ^{15}N-labeled proteins over the temperature range studied such that the exchange process quantified by titration and dispersion data must involve at least two bound conformations.

Although the equations that describe chemical exchange in a relaxation dispersion experiment can be expressed in terms of rates of interconversion and the populations of the interconverting species[22,29,31] that might then be used as fitting parameters, we prefer to fit the temperature-dependent dispersion data recorded here in terms of thermodynamic parameters, such as entropy/enthalpy differences between states as well as activation entropies/enthalpies, as discussed previously[22] and in detail in Materials and Methods. Temperature-dependent populations and rates can then be readily calculated from the thermodynamic and activation parameters that form the primary fitting variables.

The extraction of reliable thermodynamic/activation parameters describing three-state binding based on titration profiles or relaxation dispersion data alone is complicated, since each type of data is already well fit to a two-state model that requires fewer adjustable parameters. For example, in the case of a two-state model, entropy and enthalpy differences between bound and free states, ΔH and ΔS (two parameters), are required to fit the temperature-dependent dispersion data, while for the three-state model, four parameters, corresponding to enthalpy and entropy changes upon formation of $(PL)_i$, ΔH_i and ΔS_i ($i=1, 2$), are needed. As described in detail in Materials and Methods, the 'missing' two thermodynamic parameters that are necessary for the three-state model can be obtained by noting that the apparent two-state dissociation constant $K_{d,titr}$ that is obtained from titration is given by

$$K_{d,titr}^{-1} = K_{d1}^{-1} + K_{d2}^{-1} \tag{1}$$

and that the calorimetric association enthalpy, $\Delta H_{cal}=0.62\pm0.17$ kcal/mol, measured from ITC,[4] can be used to define the temperature dependence of $K_{d,titr}$ according to the van't Hoff relation,

$$\Delta H_{cal} = RT^2 d\ln\left(K_{d1}^{-1} + K_{d2}^{-1}\right)/dT, \tag{2}$$

from which it follows that $dK_{d,titr}/dT=-0.7\pm0.2$ μM/K at 25 °C. In Eqs. (1) and (2), the dissociation constant for $(PL)_i$ is given by $K_{di}=\exp((\Delta H_i - T\Delta S_i)/(RT))$ ($i=1,2$), where R is the universal gas constant and T is the absolute temperature. In principle, the temperature dependence of $K_{d,titr}$ could also be obtained by repeating the titration experiments recorded at 25 °C at a number of additional temperatures. In practice, however, the small temperature dependence noted from the ITC data implies that over a temperature range of 10–15 °C that might be used for NMR data collection, $K_{d,titr}$ values would change by only 7–10 μM, well below experimental accuracy. Furthermore, as the temperature is lowered, the exchange becomes slower such that it lies outside the fast-exchange regime, leading to severe line broadening as a function of added ligand that significantly compromises the quality of spectra. We have chosen the ITC approach instead, although an accurate value of K_d cannot be obtained from the calorimetric data because of the low ΔH_{cal} value and the low affinity of the complex that makes it difficult to titrate to completion at the protein concentrations used. Fortunately, the ΔH_{cal} value alone (obtained by fitting the ITC data using $K_{d,titr}$) provides the 'missing' information that allows extraction of the thermodynamic and activation parameters describing the three-state binding reaction from fits of the NMR data (see below and Materials and Methods).

A scenario similar to that described above in the context of extracting thermodynamic parameters occurs in the extraction of chemical shift differences in that, here, too, information additional to that provided by relaxation dispersion is required. In the two-state binding model, each residue-specific relaxation dispersion profile is described by a single chemical shift difference, $\Delta\varpi_{disp}$, corresponding to the difference in shifts between free and bound conformers. In contrast, in the case of a three-state association process, two chemical shift differences are necessary, $\Delta\varpi_{B_1F}=\varpi_{B_1}-\varpi_F$ and $\Delta\varpi_{B_2F}=\varpi_{B_2}-\varpi_F$, where F, B_1, and B_2 denote protein P in the free state, in complex $(PL)_1$, and in complex $(PL)_2$, respectively. However, the chemical shift differences required to describe a three-state binding reaction, $\Delta\varpi_{B_1F}$ and $\Delta\varpi_{B_2F}$, can be directly calculated by combining $\Delta\varpi_{titr}$ that was obtained from titration measurements at 25 °C and $\Delta\varpi_{disp}$ from dispersion data:

$$\begin{aligned}\Delta\varpi_{disp} &= \varpi_{B_2} - (p_F\varpi_F + p_{B_1}\varpi_{B_1})/(p_F + p_{B_1}) \\ &= \Delta\varpi_{B_2F} - p_{B_1}\Delta\varpi_{B_1F}/(p_F + p_{B_1}),\end{aligned} \tag{3}$$

$$\begin{aligned}\Delta\varpi_{titr} &= (p_{B_1}\varpi_{B_1} + p_{B_2}\varpi_{B_2})/(p_{B_1} + p_{B_2}) - \varpi_F \\ &= (p_{B_1}\Delta\varpi_{B_1F} + p_{B_2}\Delta\varpi_{B_2F})/(p_{B_1} + p_{B_2})\end{aligned} \tag{4}$$

where p_F, p_{B_1} and p_{B_2} are equilibrium populations of states F, B_1, and B_2, respectively, that are calculated from the three-state thermodynamic parameters at $T=25$ °C. As described in detail in Materials and Methods, the parameters of the ubiquitin–SH3-C binding reaction were extracted by a global fit of the

CPMG dispersion data using a three-state model that enforces Eqs. (1), (2), and (4) assuming that (i) the chemical shift differences $\Delta\varpi_{B_1F}$ and $\Delta\varpi_{B_2F}$ are independent of temperature and (ii) the temperature dependencies of the rates of interconversion between states follow transition-state theory. Note that identical $\Delta\varpi_{B_1F}$, $\Delta\varpi_{B_2F}$, and *equilibrium* entropies/enthalpies [ΔH_i and ΔS_i (i=1,2)] are obtained for both the consecutive and parallel binding models (see below and Materials and Methods).

Association kinetics and thermodynamics

Figure 3 shows the populations of exchanging states, exchange rate constants, and changes in thermodynamic parameters between states that are obtained in the analysis of the ^{15}N CPMG relaxation dispersion data measured on ^{15}N-labeled ubiquitin–unlabeled SH3-C and ^{15}N-labeled SH3-C–unlabeled ubiquitin samples using the three-state consecutive binding model. Results from analyses of both samples show that p_{B_2} decreases with temperature and is between 3% and 4% (Fig. 3a), while the total fraction of bound protein is essentially temperature independent (~10%). Very similar exchange rate constants $k_{ex,B_1B_2}=k_{B_1B_2}+k_{B_2B_1}$ describing the interconversion $(PL)_1 \underset{k_{B_2B_1}}{\overset{k_{B_1B_2}}{\rightleftharpoons}} (PL)_2$, are obtained from measurements on the separate samples (Fig. 3b), increasing from 2000 s^{-1} at 7.2 °C to over 6000 s^{-1} at 24.8 °C. Recall that at all temperatures interconversions between P and $(PL)_1$ are fast such that relaxation dispersion data are well described by a model of two-state exchange.

The temperature-dependent dispersion data are fit to extract the entropic (TS) and enthalpic (H) contributions to the free-energy (G) profiles that describe ubiquitin–SH3-C association. In what follows, we have fit each set of dispersions (those for ^{15}N-labeled ubiquitin and those for ^{15}N-labeled SH3-C) independently to generate separate G, TS, and H profiles that can then be used for cross-validation. Panels (c) and (d) of Fig. 3 plot the energy diagram for the three-state consecutive binding process at 25 °C. Very similar free-energy profiles are obtained from analysis of the two sets of dispersion data, with differences in TS and H for $(PL)_2$ resulting from the somewhat different temperature dependencies of p_{B_2} that emerge from fits of the two sets of dispersions (Fig. 3a). In principle, the p_{B_2} *versus* temperature profiles should be identical, and we are uncertain as to the origin of the difference. The observed differences may reflect inaccuracies in the fits of the SH3-C dispersion data resulting from (i) only half the number of high-quality SH3-C dispersion profiles reporting on the

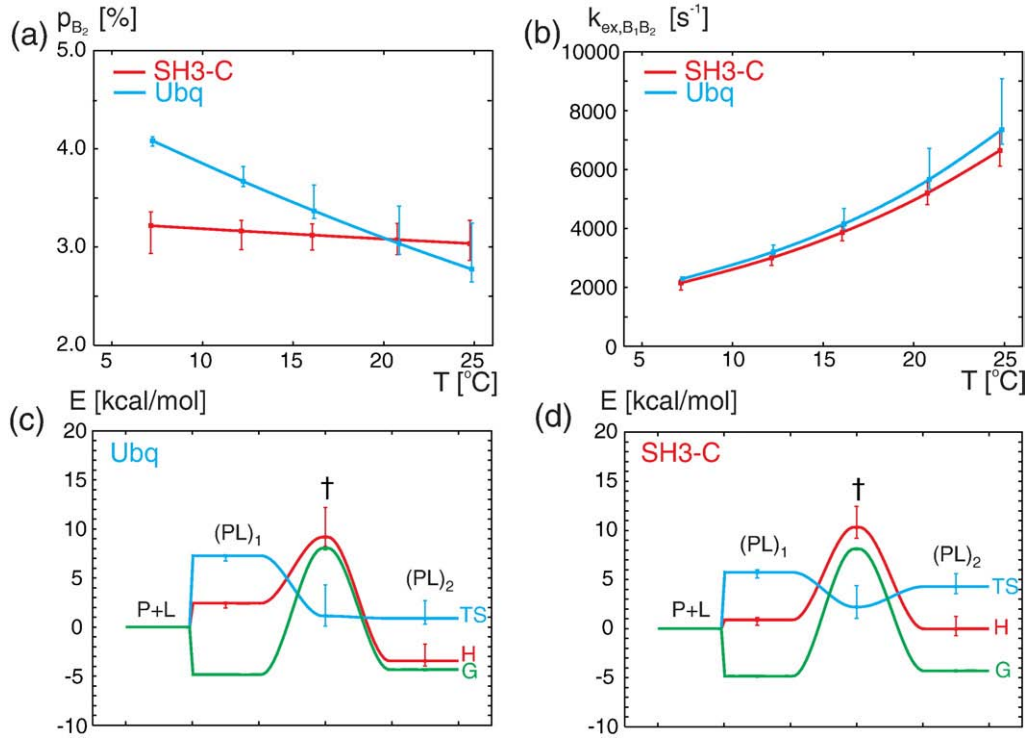

Fig. 3. Parameters of the three-state exchange model P + L ↔ $(PL)_1$ ↔ $(PL)_2$ describing the binding of ubiquitin and SH3-C. (a) Temperature dependencies of fractional populations of $(PL)_2$, p_{B_2}, and of (b) the exchange rate constant for interconversion between $(PL)_1$ and $(PL)_2$, $k_{ex,B_1B_2}=k_{B_1B_2}+k_{B_2B_1}$, obtained from global fits of ^{15}N CPMG dispersion data. (c and d) Profiles of free energy, G (green), along with enthalpic, H (red), and entropic, TS (blue), contributions to G (at 25 °C). Results from analysis of data recorded on samples of ^{15}N-labeled ubiquitin (1.0 mM)/unlabeled SH3-C (0.11 mM) are shown in (c) and indicated by blue lines in (a) and (b); those from ^{15}N-labeled SH3-C (1.2 mM)/unlabeled ubiquitin (0.15 mM) are shown in (d) and indicated by red lines in (a) and (b). Activation parameters are only obtained for the interconversion between $(PL)_1$ and $(PL)_2$ (see the text).

binding event relative to the case for ubiquitin and (ii) $\Delta\varpi_{disp}$ values for SH3-C that are somewhat smaller on average than the corresponding values for ubiquitin, that make it more difficult to separate p_{B_2} from $\Delta\varpi_{disp}$ in this case, especially at higher temperatures. In any event, the *TS* and *H* profiles of Fig. 3c and d are qualitatively similar and both establish that formation of $(PL)_1$ is accompanied by an increase in both entropy and enthalpy. $(PL)_2$ in turn is enthalpically stabilized but entropically destabilized with respect to $(PL)_1$, leading to a very slight (~0.5 kcal/mol) increase in free energy relative to $(PL)_1$. The barrier between $(PL)_1$ and $(PL)_2$ (based on the consecutive binding model) is enthalpic at 25 °C, likely pointing to conformational rearrangements of the binding surfaces of P and L that must occur prior to the formation of $(PL)_2$.

The thermodynamic parameters that have been obtained are in keeping with expectations based on a model of protein association put forth by Ross and Subramanian.[32] According to their scheme, individually hydrated species first associate to form a complex in which the hydration layers of each binding partner are 'disrupted,' leading to an increase in entropy and a concomitant increase in enthalpy that reflects the loosening of water–hydrophobe interactions. Values of ΔH and $\Delta S>0$ that are predicted are observed for the $P+L\leftrightarrow(PL)_1$ association studied here. Subsequently, in a second step, formation of short-range contacts, including van der Waals interactions and hydrogen bonds, occurs, along with immobilization of the binding surface, leading to decreases in both enthalpy and entropy that are again consistent with what has been measured here for the transition from $(PL)_1$ to $(PL)_2$.

It is worth emphasizing that it is not possible to distinguish between the parallel and consecutive three-state binding models, since the experimental data are equally well fitted by both schemes, nor is it possible to conclude that these are the only models that are consistent with the data. If the interchange between P and $(PL)_1$ could be slowed such that conversion was outside the fast-exchange limit, then the dispersion data could very likely distinguish the two binding scenarios. Fortunately, as mentioned above, the two models result in identical equilibrium thermodynamic parameters and chemical shift differences between states. The energy profiles obtained for the parallel binding model are shown in Fig. 4, and they differ from those generated for the consecutive model only in the placement of states of P+L and $(PL)_1$ along the binding pathway.

Notably, the parallel binding model predicts significantly different association rates k_{on1} and k_{on2} for the formation of $(PL)_1$ and $(PL)_2$. Since the dispersion data over the complete temperature range are well fit to a two-state binding model, one of the two binding processes, $P+L\underset{k_{off1}}{\overset{k_{on1}}{\rightleftharpoons}}(PL)_1$, must be fast on the NMR time scale, with the second process, $P+L\underset{k_{off2}}{\overset{k_{on2}}{\rightleftharpoons}}(PL)_2$, in the intermediate-exchange regime

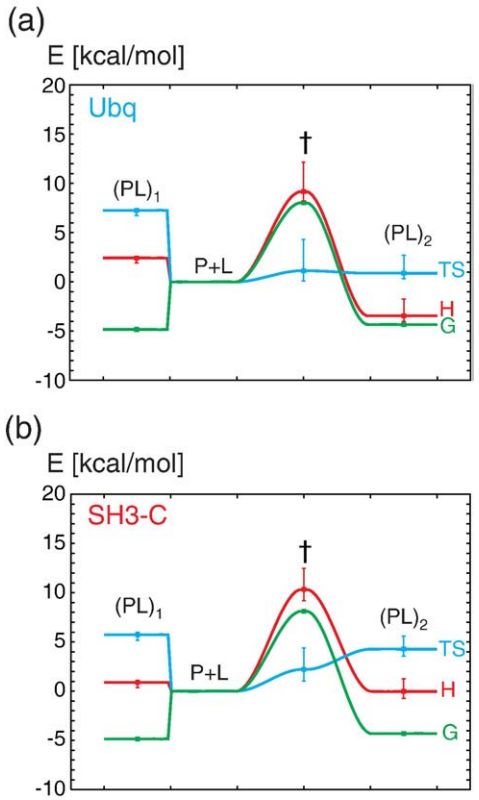

Fig. 4. Profiles of free energy, *G* (green), along with enthalpic, *H* (red), and entropic, *TS* (blue), contributions to *G* (at 25 °C) for the parallel binding model $(PL)_1\leftrightarrow P+L\leftrightarrow(PL)_2$. Results from analysis of data recorded on samples of ^{15}N-labeled ubiquitin (1.0 mM)/unlabeled SH3-C (0.11 mM) are shown in (a); those from ^{15}N-labeled SH3-C (1.2 mM)/unlabeled ubiquitin (0.15 mM) are shown in (b).

at 5–15 °C. A k_{on2} value of $\sim 7\times10^6$ M^{-1} s^{-1} at 25 °C is obtained from a combined analysis of the titration and relaxation dispersion data recorded on either ^{15}N-labeled ubiquitin or ^{15}N-labeled SH3-C samples, which is faster than rates of 10^5–10^6 M^{-1} s^{-1} that are expected for diffusion-controlled association.[33] Although k_{on1} cannot be determined with precision, since the $P+L\leftrightarrow(PL)_1$ binding event is fast, it must be at least an order of magnitude faster than k_{on2}. Within the context of the parallel binding model, $k_{on1}\gg k_{on2}$ reflects the fact that significantly more conformational changes are involved in the formation of $(PL)_2$ relative to $(PL)_1$. This is consistent with a more loosely formed interface for $(PL)_1$, which is also suggested by a comparison of the relative thermodynamic parameters of $(PL)_1$ and $(PL)_2$. The kinetic and thermodynamic parameters are summarized in Tables 1 and 2.

Insights into the structural features of $(PL)_1$ and $(PL)_2$ based on NMR chemical shifts

The chemical shift differences $\Delta\varpi_{B_1F}=\varpi_{B_1}-\varpi_F$ and $\Delta\varpi_{B_2F}=\varpi_{B_2}-\varpi_F$ obtained from a combined analysis of titration and relaxation dispersion data

Table 1. Fractional populations of $(PL)_1$ and $(PL)_2$, p_{B_1} and p_{B_2}, that are measured from fits of ^{15}N relaxation dispersion profiles

	Ubiquitin[a]				SH3-C[b]			
T (°C)	p_{B_1} (%)	p_{B_2} (%)	$k_{B_1B_2}+k_{B_2B_1}$ (s^{-1})	$k_{FB_2}+k_{B_2F}$ (s^{-1})	p_{B_1} (%)	p_{B_2} (%)	$k_{B_1B_2}+k_{B_2B_1}$ (s^{-1})	$k_{FB_2}+k_{B_2F}$ (s^{-1})
7.2	5.04 (5.04±0.05)	4.08 (4.08±0.05)	2290 (2281±46)	1322 (1317±18)	7.27 (7.35±0.21)	3.22 (3.15±0.21)	2147 (2085±172)	1542 (1508±84)
12.2	5.45 (5.40±0.11)	3.67 (3.72±0.10)	3205 (3274±169)	1993 (2015±67)	7.36 (7.40±0.15)	3.16 (3.12±0.15)	3000 (2941±193)	2173 (2138±99)
16.1	5.76 (5.66±0.18)	3.37 (3.47±0.17)	4156 (4327±352)	2719 (2781±148)	7.42 (7.44±0.13)	3.12 (3.10±0.13)	3866 (3819±242)	2816 (2786±128)
20.8	6.11 (5.97±0.25)	3.04 (3.17±0.24)	5665 (6032±689)	3911 (4059±314)	7.50 (7.49±0.16)	3.08 (3.08±0.16)	5201 (5192±377)	3815 (3800±202)
24.8	6.39 (6.22±0.30)	2.77 (2.94±0.30)	7353 (7973±1115)	5284 (5551±539)	7.56 (7.53±0.20)	3.04 (3.07±0.20)	6649 (6699±580)	4904 (4913±309)

Exchange rates $k_{ex,B_1B_2}=k_{B_1B_2}+k_{B_2B_1}$ and $k_{ex,FB_2}=k_{FB_2}+k_{B_2F}$, which are relevant for the $P+L\leftrightarrow(PL)_1\leftrightarrow(PL)_2$ and $(PL)_1\leftrightarrow P+L\leftrightarrow(PL)_2$ models, respectively, are listed. Errors were estimated using a jackknife procedure (in parentheses are the mean±SD values of the obtained distributions).

[a] Recorded on a sample of ^{15}N-ubiquitin, unlabeled SH3-C, with approximately 10% mole fraction SH3-C.

[b] Recorded on a sample of ^{15}N-labeled SH3-C with unlabeled ubiquitin (~10%).

provide qualitative probes of structure in $(PL)_1$ and $(PL)_2$. Panels (a) and (b) of Fig. 5 plot $\Delta\varpi_{B_1F}$ (black bars) and $\Delta\varpi_{B_2F}$ (red bars) *versus* residue number for ubiquitin (a) and SH3-C (b), with the values listed in Tables 3 and 4. It is clear that the formation of $(PL)_2$ is accompanied by pronounced ^{15}N chemical shift changes in both proteins, while in $(PL)_1$, the chemical shifts of both partners are, for the most part, similar to those in the corresponding unbound states. Notable exceptions include the amides of Gly47–Gln49, His68, and Leu71 in ubiquitin and Ile275, Phe276, Asn282, Asp283, Trp306 (both amide and $N^{\varepsilon 1}$), and Asp320 in SH3-C for which $\Delta\varpi_{B_1F}$ values over 0.5 ppm are obtained (Fig. 5a and b). Large binding-induced changes in ^{15}N chemical shifts are consistent with significant conformational rearrangements and/or changes in residue packing at the binding interface, such as movement of aromatic or polar/charged side chains.[35] Thus, the observed chemical shift differences provide evidence that formation of $(PL)_2$ involves more pronounced conformational rearrangements and increasing packing of the binding surface than is the case for $(PL)_1$. This is consistent with the higher enthalpy and entropy of $(PL)_1$ relative to $(PL)_2$ that presumably result from fewer favorable contacts and increased mobility of the binding interface in $(PL)_1$ (see Figs. 3 and 4). The similar stabilities of $(PL)_1$ and $(PL)_2$, despite the increased number of contacts in $(PL)_2$, emphasize the role of entropy/enthalpy compensation in the formation of these distinct binding modes and serve as a reminder of the important role of entropy in the formation of complexes,[32] despite the emphasis on enthalpy that emerges from the static structures produced by NMR or X-ray crystallography.

Ubiquitin interacts with its binding partners through a hydrophobic patch involving Ile44 flanked by polar/charged residues, and mutation of Ile44 in most cases completely abolishes binding.[21] In turn, all ubiquitin binding domains contain a complementary hydrophobic patch flanked by residues with negative electrostatic potential. In the case of SH3-C, a critical residue is Phe322, which forms extensive contacts with Ile44 and His68 of ubiquitin.[20] Other important contacts include interactions of SH3-C Phe276 with ubiquitin His68 and Ile44 and those of SH3-C Trp306 and Pro319 with ubiquitin Leu8 and Val70, respectively.

A comparison of $\Delta\varpi_{B_1F}$ and $\Delta\varpi_{B_2F}$ can be used to highlight some of the structural features of the complexes $(PL)_1$ and $(PL)_2$. Panels (c) and (d) of Fig. 5 show values of $\Delta\varpi_{B_1F}$ (c) and $\Delta\varpi_{B_2F}$ (d) mapped onto the structures of ubiquitin and SH3-C as they exist in complex, based on a recent NMR structural study.[20] In Fig. 5e, the interface is shown with residues color coded according to the ratio $\Delta\varpi_{B_1F}/\Delta\varpi_{B_2F}$. Qualitatively, residues for which $\Delta\varpi_{B_1F}/\Delta\varpi_{B_2F}=\sim 0$ are those where 'bound'-state structural features formed in $(PL)_2$ are not present in $(PL)_1$. Conversely, residues with higher than average $\Delta\varpi_{B_1F}/\Delta\varpi_{B_2F}$ ratios and where $\Delta\varpi_{B_1F}$ and $\Delta\varpi_{B_2F}$

Table 2. Free energy, *G*, along with enthalpic, *H*, and entropic, *TS*, contributions to *G* (calculated at 25 °C) for states F, B_1, and B_2 corresponding to apo-P and bound states $(PL)_1$ and $(PL)_2$, respectively, for the ubiquitin–SH3-C binding reaction

	Ubiquitin[a]			SH3-C[b]		
State	*H* (kcal/mol)	*TS* (kcal/mol)	*G* (kcal/mol)	*H* (kcal/mol)	*TS* (kcal/mol)	*G* (kcal/mol)
F	0	0	0	0	0	0
B_1	2.43 (2.23±0.29)	7.26 (7.04±0.32)	−4.83 (−4.81±0.03)	0.88 (0.74±0.39)	5.73 (5.58±0.40)	−4.85 (−4.84±0.02)
†	9.17 (10.19±1.98)	1.13 (2.21±2.10)	8.04 (7.98±0.12)	10.33 (10.83±1.63)	2.21 (2.72±1.68)	8.12 (8.11±0.07)
B_2	−3.45 (−2.86±1.13)	0.88 (1.50±1.19)	−4.33 (−4.36±0.06)	−0.03 (0.26±0.99)	4.28 (4.57±1.02)	−4.31 (−4.31±0.04)

Errors in thermodynamic parameters were estimated using a jackknife procedure (shown in parentheses are the mean±SD values of the distributions obtained from the jackknife fit). The thermodynamic parameters are independent of the choice of the three-state binding model.

[a] Obtained from fits of ^{15}N relaxation dispersion data recorded on a sample of ^{15}N-labeled ubiquitin and unlabeled SH3-C, with approximately 10% mole fraction of SH3-C. The dissociation constants for B_1 and B_2 are $K_{d1}=0.29$ mM and $K_{d2}=0.67$ mM, respectively.

[b] As in (a), but SH3-C is ^{15}N labeled and ubiquitin is unlabeled. $K_{d1}=0.28$ mM; $K_{d2}=0.69$ mM.

are >0.5 ppm are those where interactions that are present in $(PL)_2$ are at least partially formed in $(PL)_1$. In the context of the consecutive binding model, the $\Delta\varpi_{B_1F}/\Delta\varpi_{B_2F}$ ratios can be used as qualitative indicators that 'map' the formation of contacts during binding, with larger than average $\Delta\varpi_{B_1F}/\Delta\varpi_{B_2F}$ ratios reflecting 'hot spots' of association that are already formed in $(PL)_1$ and values of $\Delta\varpi_{B_1F}/\Delta\varpi_{B_2F}$ that are close to zero indicating interactions formed in $(PL)_2$ but not yet emerged in $(PL)_1$.

Surprisingly, both Ile44 (and neighboring Phe45) of ubiquitin and Phe322 of SH3-C, identified as key residues for ubiquitin–SH3 association, have small $\Delta\varpi_{B_1F}$ values and low $\Delta\varpi_{B_1F}/\Delta\varpi_{B_2F}$ ratios, suggesting that the network of contacts involving these residues is not fully formed in $(PL)_1$. Another region of interest comprising Trp306 (and neighboring residues) of SH3-C and Leu8 of ubiquitin also has small $\Delta\varpi_{B_1F}$ values and low $\Delta\varpi_{B_1F}/\Delta\varpi_{B_2F}$ ratios for the backbone amide groups, although higher $\Delta\varpi_{B_1F}$ (0.79 ppm) and $\Delta\varpi_{B_1F}/\Delta\varpi_{B_2F}$ (0.55) values are observed for $^{15}N^{\varepsilon 1}$ of Trp306, suggesting that the side chain of this residue may form some interactions in $(PL)_1$. In contrast, higher than average $\Delta\varpi_{B_1F}/\Delta\varpi_{B_2F}$ ratios with $\Delta\varpi_{B_1F}>0.5$ ppm were obtained for the backbone amides of Phe276 (and neighboring Ile275) located in the beginning of the RT loop of SH3-C and for His68 and Gly47–Gln49 in ubiquitin that flank the side chain of Phe276 from both sides (Fig. 5c and e). This region is thus relatively well formed in $(PL)_1$ and, in the context of the consecutive binding model, would be considered as a 'hot spot' that forms early on in the association of SH3-C and ubiquitin. Two more residues in SH3-C with pronounced $\Delta\varpi_{B_1F}$ and high $\Delta\varpi_{B_1F}/\Delta\varpi_{B_2F}$ values are Asn282 and Asp283, which are located opposite to the C-terminal region of ubiquitin. Note that the penultimate residue in ubiquitin, Arg74, also has a relatively high $\Delta\varpi_{B_1F}/\Delta\varpi_{B_2F}$ value.

In summary, we have presented a binding study on ubiquitin–CIN85 SH3-C in which NMR titration and relaxation dispersion data that independently are well fit by a two-state binding model can be fit together only if a more complex three-state binding model is chosen. A combined analysis establishes that there are two binding modes with similar stabilities and similar binding interfaces that have distinct levels of organization. Modular domains of regulatory proteins have evolved to allow versatile interactions involving multiple binding partners,[36,37] often by utilizing the same binding surface. This is the case for the interaction between the SH3-C of CIN85 and ubiquitin that involves the 'classical' binding sites of these proteins. The distinct binding modes that have been quantified in this study emphasize the interplay between entropy and enthalpy in stabilizing complexes in which the level of organization of the binding interface can vary significantly. This provides yet another layer of complexity to fine-tune molecular interactions.

Materials and Methods

Protein expression and purification

^{15}N-labeled samples of ubiquitin (residues 1–76) and the third SH3 domain of the CIN85 adaptor protein (SH3-C, residues 267–328) were expressed and purified as described previously.[20] Proteins were expressed in *Escherichia coli* BL21(DE3) cells in M9 minimal medium with $^{15}NH_4Cl$ and $[^{12}C_6]$glucose as the sole nitrogen and carbon sources, respectively, while unlabeled proteins were grown in LB medium.

NMR titration experiments

Titration of ^{15}N-labeled ubiquitin with the SH3-C domain was performed at 25 °C by gradually adding a stock solution of concentrated unlabeled SH3-C into a 0.14 mM ^{15}N-labeled ubiquitin sample as described previously.[20] Similarly, titration of ^{15}N-labeled SH3-C with ubiquitin was performed by adding unlabeled ubiquitin to a 0.5 mM sample of ^{15}N-labeled SH3-C. To monitor binding-induced changes in ^{15}N chemical shifts, we collected ^1H–^{15}N heteronuclear single-quantum coherence spectra at each point in the titration. Changes in ^{15}N chemical shifts as a function of added ligand (titration profiles) for $n_r=30$ NH groups of ^{15}N-labeled ubiquitin ($n_r=23$ NH groups of ^{15}N-labeled SH3-C) were fit together

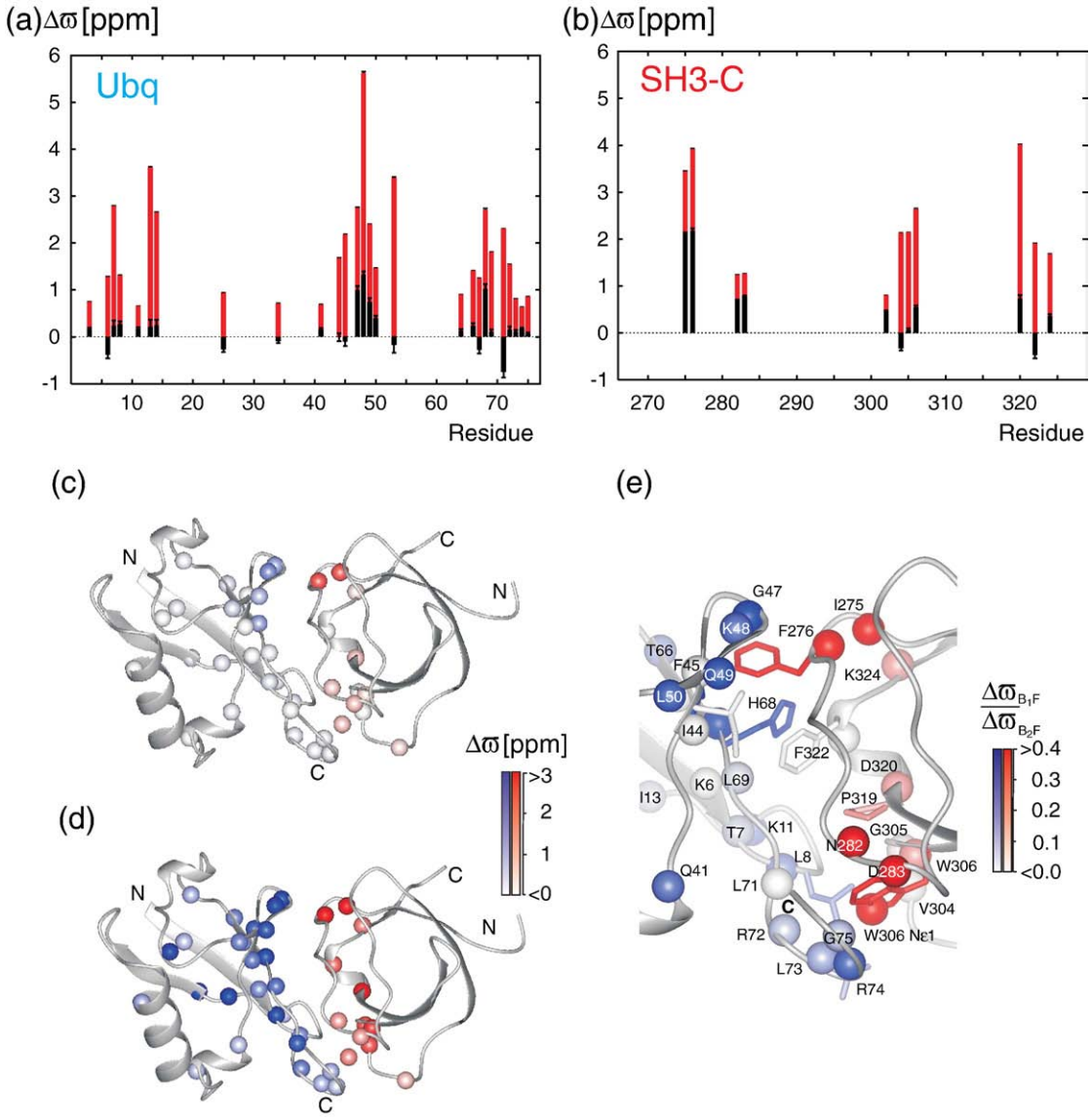

Fig. 5. Chemical shifts probe structural features of $(PL)_1$ and $(PL)_2$. Chemical shift differences $\Delta\varpi_{B_1F}$ (black) and $\Delta\varpi_{B_2F}$ (red) obtained from the analysis of ^{15}N CPMG dispersion data recorded on samples of ^{15}N-labeled ubiquitin/unlabeled SH3-C (a) and ^{15}N-labeled SH3-C/unlabeled ubiquitin (b) based on a three-state exchange model. For clarity of presentation, absolute values of $\Delta\varpi_{B_2F}$ are plotted, while values of $\Delta\varpi_{B_1F}$ are plotted positive (negative) for $\Delta\varpi_{B_2F}\Delta\varpi_{B_1F}>0$ ($\Delta\varpi_{B_2F}\Delta\varpi_{B_1F}<0$). Color-coded values of $\Delta\varpi_{B_1F}$ and $\Delta\varpi_{B_2F}$ are mapped onto the structure of the ubiquitin–SH3-C complex in (c) and (d), respectively, where blue and red are reserved for ubiquitin and SH3-C. (e) ^{15}N $\Delta\varpi_{B_1F}/\Delta\varpi_{B_2F}$ ratios color mapped onto the interaction interface of the ubiquitin–SH3-C complex.

to a model of two-state binding, $P+L\leftrightarrow PL$, using the following equations:

$$\varpi = \varpi_F + (\varpi_B - \varpi_F)\frac{L_0 - [L]}{P_0} \quad (5)$$

and

$$[L] = \frac{1}{2}\left(\sqrt{(P_0 - L_0 + K_d)^2 + 4L_0K_d} - (P_0 - L_0 + K_d)\right), \quad (6)$$

where $K_d = [P][L]/[PL]$ is the dissociation constant; [P], [L], and [PL] are concentrations of free protein, free ligand, and the complex, respectively; P_0 and L_0 are the total concentrations of protein and ligand at each point in the titration, respectively; ϖ_F and ϖ_B are the ^{15}N chemical shifts of the ligand-free (P) and ligand-bound (PL) protein states, respectively; and ϖ is the measured chemical shift at a given [L]. The model [Eqs. (5) and (6)] include $n_{par} = 2n_r+1$ adjustable parameters: n_r values of ^{15}N chemical shifts in the free state, ϖ_F; n_r chemical shift differences between bound and free states, $\Delta\varpi_{titr} = \varpi_B - \varpi_F$; and the dissociation constant, $K_{d,titr}$. The data were fit using a script written in Mathematica software (Wolfram Research). The errors of the extracted model parameters were estimated using the covariance matrix method.[34]

NMR relaxation dispersion experiments

^{15}N relaxation dispersion measurements were performed for two protein samples (both in 50 mM phosphate buffer, pH 6.4, 150 mM NaCl, 2 mM DTT, and 90% H_2O/10% D_2O) containing (i) 1.2 mM ^{15}N-labeled SH3-C and 0.15 mM

Table 3. ^{15}N chemical shift differences for ubiquitin, $\Delta\varpi_{titr}$ and $\Delta\varpi_{disp}$, obtained from global fits of ^{15}N relaxation dispersion and titration data using two-state binding models, along with values of $\Delta\varpi_{B_1F}$ and $\Delta\varpi_{B_2F}$ that are obtained from fits of relaxation dispersion data to three-state models of binding

	Two-state model		Three-state model	
Residue	$\Delta\varpi_{titr}$ (ppm)	$\Delta\varpi_{disp}$ (ppm)	$\Delta\varpi_{B_1F}$ (ppm)	$\Delta\varpi_{B_2F}$ (ppm)
I3	−0.34±0.07	−0.73±0.03	−0.17 (−0.15±0.03)	−0.75 (−0.745±0.002)
K6	0.12±0.07	1.29±0.02	−0.38 (−0.41±0.08)	1.28 (1.274±0.005)
T7	−1.01±0.07	−2.75±0.03	−0.24 (−0.17±0.11)	−2.79 (−2.782±0.008)
L8	−0.59±0.07	−1.29±0.02	−0.27 (−0.25±0.06)	−1.31 (−1.311±0.004)
K11	−0.32±0.07	−0.64±0.03	−0.18 (−0.17±0.03)	−0.65 (−0.652±0.003)
I13	1.24±0.08	3.57±0.04	0.22 (0.11±0.15)	3.61 (3.597±0.015)
T14	0.98±0.07	2.62±0.03	0.25 (0.20±0.12)	2.65 (2.647±0.006)
N25	−0.09±0.08	−0.94±0.04	0.27 (0.31±0.06)	−0.94 (−0.935±0.002)
E34	−0.15±0.07	−0.71±0.03	0.09 (0.13±0.04)	−0.71 (−0.713±0.002)
Q41	−0.32±0.07	−0.67±0.03	−0.16 (−0.14±0.03)	−0.69 (−0.688±0.002)
R42	−0.35±0.08	—	—	—
I44	0.50±0.07	1.66 0.02	−0.01 (−0.04±0.09)	1.68 (1.674±0.002)
F45	0.59±0.07	2.16±0.03	−0.10 (−0.20±0.09)	2.18 (2.181±0.007)
G47	1.52±0.08	2.66±0.04	0.99 (0.93±0.09)	2.75 (2.748±0.017)
K48	−2.63±0.11	−5.50±0.07	−1.33 (−1.39±0.07)	−5.63 (−5.651±0.024)
Q49	−1.24±0.08	−2.34±0.03	−0.74 (−0.69±0.09)	−2.40 (−2.395±0.003)
L50	0.72±0.07	1.43±0.03	0.40 (0.37±0.06)	1.46 (1.460±0.003)
E51	0.33±0.07	—	—	—
G53	−0.91±0.07	−3.37±0.04	0.17 (0.27±0.17)	−3.39 (−3.379±0.015)
E64	0.36±0.07	0.89±0.03	0.13 (0.12±0.04)	0.90 (0.897±0.002)
T66	0.59±0.07	1.39±0.02	0.23 (0.20±0.06)	1.41 (1.406±0.002)
L67	−0.18±0.07	−1.25±0.03	0.28 (0.33±0.08)	−1.25 (−1.245±0.007)
H68	−1.54±0.08	−2.62±0.04	−1.03 (−0.96±0.09)	−2.71 (−2.707±0.027)
L69	−0.62±0.07	−1.79±0.02	−0.10 (−0.01±0.06)	−1.81 (−1.804±0.003)
V70	−1.14±0.08	—	—	—
L71	0.17±0.07	2.33±0.03	−0.75 (−0.88±0.11)	2.31 (2.300±0.004)
R72	0.57±0.07	1.52±0.02	0.15 (0.09±0.07)	1.54 (1.540±0.007)
L73	0.32±0.07	0.79±0.02	0.11 (0.09±0.03)	0.81 (0.804±0.002)
R74	−0.31±0.07	−0.62±0.02	−0.17 (−0.16±0.02)	−0.63 (−0.629±0.003)
G75	−0.30±0.07	−0.84±0.02	−0.06 (0.04±0.03)	−0.85 (0.854±0.002)

Signs of $\Delta\varpi_{titr}$ were determined from the analysis of ^{15}N NMR titration profiles, while the signs of $\Delta\varpi_{disp}$ and $\Delta\varpi_{B_2F}$ were assumed to be the same as the sign of $\Delta\varpi_{titr}$ (see Materials and Methods). Errors in ($\Delta\varpi_{titr}$,$\Delta\varpi_{disp}$) and ($\Delta\varpi_{B_1F}$,$\Delta\varpi_{B_2F}$) were estimated using the covariance matrix method and by the jackknife approach[34] (shown in parentheses are mean±SD values), respectively.

Table 4. ^{15}N chemical shift differences for SH3-C

	Two-state model		Three-state model	
Residue	$\Delta\varpi_{titr}$ (ppm)	$\Delta\varpi_{disp}$ (ppm)	$\Delta\varpi_{B_1F}$ (ppm)	$\Delta\varpi_{B_2F}$ (ppm)
I275	2.49±0.05	3.28±0.07	2.11 (2.11±0.03)	3.44 (3.456±0.010)
F276	−2.68±0.04	−3.76±0.08	−2.18 (−2.18±0.05)	−3.92 (−3.917±0.011)
A280	−0.63±0.03	—	—	—
N282	0.85±0.02	1.18±0.03	0.69 (0.69±0.02)	1.24 (1.234±0.005)
D283	0.92±0.02	1.20±0.03	0.79 (0.79±0.01)	1.26 (1.256±0.003)
D284	−0.38±0.02	—	—	—
L286	0.48±0.02	—	—	—
K289	0.30±0.02	—	—	—
V294	0.37±0.02	—	—	—
C301	0.29±0.02	—	—	—
I302	−0.56±0.06	−0.76±0.03	−0.47 (−0.47±0.01)	−0.80 (−0.799±0.002)
D303	−0.58±0.02	—	—	—
V304	−0.38±0.02	−2.15±0.04	0.33 (0.35±0.05)	−2.13 (−2.128±0.005)
G305	−0.65±0.02	−2.14±0.04	−0.05 (−0.07±0.04)	−2.14 (−2.143±0.004)
W306	−1.14±0.02	−2.60±0.05	−0.54 (−0.50±0.04)	−2.64 (−2.642±0.012)
W307	−0.55±0.02	—	—	—
E308	−0.60±0.02	—	—	—
V317	0.26±0.02	—	—	—
D320	1.67±0.05	3.96±0.09	0.73 (0.72±0.08)	4.01 (4.015±0.012)
F322	−0.21±0.02	−1.94±0.04	0.47 (0.49±0.07)	−1.91 (−1.904±0.005)
V323	0.34±0.02	—	—	—
K324	−0.74±0.04	−1.66±0.04	−0.36 (−0.36±0.03)	−1.69 (−1.685±0.004)
W306 $N^{\varepsilon 1}$	−0.98±0.02	−1.39±0.03	−0.79 (−0.78±0.03)	−1.45 (−1.447±0.003)

See the legend to Table 3.

unlabeled ubiquitin and (ii) 0.98 mM ^{15}N-labeled ubiquitin and 0.11 mM unlabeled SH3-C. The experiments were performed at five temperatures (7.2, 12.2, 16.1, 20.8, and 24.8 °C) and two or three magnetic fields (11.7 and 18.8 T for ^{15}N-labeled ubiquitin; 11.7, 14.1, and 18.8 T for ^{15}N-labeled SH3-C) using the pulse scheme of Tollinger *et al.*[38]

Relaxation dispersion profiles for $n_r = 27$ NH groups of ^{15}N-labeled ubiquitin ($n_r = 12$ NH groups of ^{15}N-labeled SH3-C) were measured at $n_f = 2$ (3) magnetic fields and $n_t = 5$ temperatures. The dispersion profiles were fit together initially to a simple two-state binding model, P + L ↔ PL, to extract chemical shift differences between bound and free states, $\Delta\varpi_{disp}$, and $K_{d,disp}$ for comparison with the corresponding values obtained from analysis of titration data. The fits assumed that (i) $\Delta\varpi_{disp} = \varpi_B - \varpi_F$ values are independent of temperature and (ii) the temperature dependencies of the association and dissociation rates, k_{on} and k_{off}, respectively, obey transition-state theory. The model includes $n_{par} = n_t n_f n_r + n_r + 4$ adjustable parameters: $n_t n_f n_r$ values of intrinsic R_2 rates assumed to be the same in the free and bound states (specific for each NH group, temperature, and field); n_r values of ^{15}N chemical shift differences, $\Delta\varpi_{disp} = \varpi_B - \varpi_F$ (specific for each NH group); and four thermodynamic parameters, including the entropy and enthalpy differences between the bound and free states, ΔH and ΔS (bound − free), and activation parameters for the dissociation process, $\Delta H^{\dagger}$ and $\Delta S^{\dagger}$ (common for all NH groups). Although the intrinsic relaxation rates are not expected to be the same for ubiquitin or SH3-C and the ubiquitin–SH3 complex, this is not expected to affect the accuracy of the extracted relaxation dispersion parameters in the case where the fraction of the minor state (complex) is small and the difference in relaxation rates is negligible relative to the chemical shift differences between exchanging states,[39] as is the situation here.

The data were fit using home-written software as described in detail elsewhere.[22] The errors of extracted model parameters were estimated using the covariance matrix method.[34]

ITC measurements

Experiments were carried out at 25 °C with a Calorimetry Sciences Corporation Model 4200 isothermal titration calorimeter. A value for the association enthalpy ΔH_{cal} for the binding reaction was measured by titrating 2.0 mM SH3-C into 0.45 or 0.95 mM samples of ubiquitin (two experiments) and *vice versa* by titrating 2.3 mM ubiquitin into 0.40 mM SH3-C (one experiment). The heat of dilution was estimated by titrating the same stock solutions into buffer. The data were analyzed with K_d fixed to 200 μM, resulting in $\Delta H_{cal} = 0.62 \pm 0.17$ kcal/mol (averaged over three measurements), which corresponds to $dK_{d,titr}/dT = -0.7$ μM/K at 25 °C.

Analysis of relaxation dispersion data using titration and ITC results

As described in Results and Discussion, the inconsistency between the apparent two-state parameters obtained from relaxation dispersion and titration data (dissociation constants and chemical shift differences between states) establishes that the binding mechanism is more complex than that described by P + L ↔ PL and that it involves the formation of at least two alternative binding modes, $(PL)_1$ and $(PL)_2$. A number of binding models that are consistent with both the ITC, titration, and relaxation dispersion data include P + L ↔ $(PL)_1$ ↔ $(PL)_2$ (consecutive binding) and $(PL)_1$ ↔ P + L ↔ $(PL)_2$ (parallel binding). NMR titration and ITC data can be described by a process where $(PL)_1$ and $(PL)_2$ are in rapid equilibrium, P + L ↔ {$(PL)_1$,$(PL)_2$}, such that it is not possible to discriminate between them. This gives rise to two-state binding that would produce a binding profile identical with that obtained with the simpler P + L ↔ PL scheme. An effective dissociation constant, referred to as $K_{d,titr}$, is obtained that is given by

$$K_{d,titr} = \frac{[P][L]}{[(PL)_1] + [(PL)_2]} \tag{7}$$

In contrast, the relaxation dispersion data report on an apparent two-state process, {P,$(PL)_1$} ↔ $(PL)_2$, where it is not possible to distinguish between protein P in the free state or in one of the complexes [arbitrarily chosen to be $(PL)_1$]. Thus, relaxation dispersion data are consistent with either P + L ↔ $(PL)_1$ ↔ $(PL)_2$ or $(PL)_1$ ↔ P + L ↔ $(PL)_2$ binding models where (i) the P + L ↔ $(PL)_1$ interconversion is fast on the NMR time scale at all temperatures and (ii) $(PL)_1$ ↔ $(PL)_2$ (consecutive binding model) or P + L ↔ $(PL)_2$ (parallel binding model) falls into the intermediate-exchange regime at low temperatures (5–15 °C), where pronounced CPMG dispersion profiles are observed.

The parameters of the three-state binding models can be readily calculated by minimization of the following χ^2 target function:

$$\chi^2(\zeta) = \sum \frac{\left(R_{2,eff}^{clc}(\zeta) - R_{2,eff}^{exp}\right)^2}{\left(\Delta R_{2,eff}^{exp}\right)^2}, \tag{8}$$

where $R_{2,eff}^{clc}(\zeta)$ is the calculated relaxation rate from numerical solution of the Bloch–McConnell equations[40] for magnetization evolution during the CPMG sequence, $\zeta = \{x_1, \ldots, x_{n_{par}}\}$ is the set of adjustable model parameters described below, n_{par} is the number of model parameters, $R_{2,eff}^{exp}$ is the experimental value with error $\Delta R_{2,eff}^{exp}$, and the summation is over the number of experimental data points, n_{dat}. Theoretical values of $R_{2,eff}^{clc}$ were calculated according to

$$R_{2,eff}^{clc} = -\frac{1}{4n\delta} \ln \frac{M_F(4n\delta)}{M_F(0),} \tag{9}$$

where

$$\mathbf{M}_{\pm}(4n\delta) = (\exp(\mathbf{A}_{\pm}\delta)\exp(\mathbf{A}_{\mp}\delta)\exp(\mathbf{A}_{\mp}\delta)\exp(\mathbf{A}_{\pm}\delta))^n \mathbf{M}_{\pm}(0), \tag{10}$$

$T_{CP} = 4n\delta$ is the duration of the constant time $(\delta\text{–}180°_x\text{–}\delta)_{2n}$ CPMG pulse train with $2n$ refocusing $180°_x$ pulses [applied with frequency $\nu_{CPMG} = 1/(4\delta)$], $\mathbf{M}(t) = \mathbf{M}_+(t) + \mathbf{M}_-(t)$ is the magnetization vector given by $[M_F(t), M_{B_1}(t), M_{B_2}(t)]^T$ in the case of three-site exchange between states F, B_1, and B_2 [here, F, B_1, and B_2 refer to free protein P, $(PL)_1$, $(PL)_2$, respectively], $\mathbf{M}(0)$ is the initial magnetization vector set to the fractional populations of each of the states $(p_F, p_{B_1}, p_{B_2})^T$ (here, T denotes transpose), and $\mathbf{M}_{\pm} = \mathbf{M}_x \pm i\mathbf{M}_y$, $i = \sqrt{-1}$. For a general 'triangular' three-site exchange model where interconversions between all states are allowed, the 3×3 evolution matrices $\mathbf{A}_+$ and $\mathbf{A}_-$ are given by

$$\mathbf{A}_{\pm} = \begin{pmatrix} -R_{2F} - k_{FB_1} - k_{FB_2} & k_{B_1F} & k_{B_2F} \\ k_{FB_1} & -R_{2B_1} - k_{B_1F} - k_{B_1B_2} \pm i\Delta\omega_{B_1F} & k_{B_2B_1} \\ k_{FB_2} & k_{B_1B_2} & -R_{2B_2} - k_{B_2F} - k_{B_2B_1} \pm i\Delta\omega_{B_2F} \end{pmatrix}, \tag{11}$$

where k_{kl} denotes the rate of transition from state k to state l (k, l=F, B_1, and B_2), R_{2k} is the intrinsic transverse relaxation rate in state k, $\Delta\omega_{kl}=\omega_N\Delta\varpi_{kl}$ is the frequency difference between state k and state l (in radians per second), and ω_N is the Larmor frequency of the ^{15}N nucleus.

The rates and populations can in turn be recast in terms of the following fitting parameters:

$$k_{B_1F} = k_{off1} = (k_BT/h)\exp\left(-\Delta G_1^{\dagger}/(RT)\right), \tag{12}$$

$$k_{FB_1} = k_{on1}[L] = (k_{off1}/K_{d1})[L] = (k_BT/h)\exp\left(-\left(\Delta G_1 + \Delta G_1^{\dagger}\right)/(RT)\right)[L],$$

$$k_{B_2F} = k_{off2} = (k_BT/h)\exp\left(-\Delta G_2^{\dagger}/(RT)\right),$$

$$k_{FB_2} = k_{on2}[L] = (k_{off2}/K_{d2})[L] = (k_BT/h)\exp\left(-\left(\Delta G_2 + \Delta G_2^{\dagger}\right)/(RT)\right)[L],$$

$$k_{B_2B_1} = (k_BT/h)\exp\left(-\Delta G^{\dagger}/(RT)\right),$$

$$k_{B_1B_2} = k_{B_2B_1}(K_{d1}/K_{d2}) = (k_BT/h)\exp\left(-\left(\Delta G_2 - \Delta G_1 + \Delta G^{\dagger}\right)/(RT)\right),$$

where $K_{di}=\exp(\Delta G_i/(RT))$, $k_{offi}=(k_BT/h)\exp(-\Delta G_i^{\dagger}/(RT))$, and $k_{oni}=(k_{offi}/K_{di})$ are the equilibrium dissociation constant, the dissociation rate constant, and the bimolecular association rate constant for the $(PL)_i$ complex (i=1,2), respectively; $\Delta G_i=\Delta H_i-T\Delta S_i$, ΔH_i, and ΔS_i are equilibrium free-energy, entropy, and enthalpy changes upon formation of $(PL)_i$, respectively; $\Delta G_i^{\dagger}=\Delta H_i^{\dagger}-T\Delta S_i^{\dagger}$, $\Delta H_i^{\dagger}$, and $\Delta S_i^{\dagger}$ are the activation parameters for the $(PL)_i\rightarrow P+L$ dissociation process; $\Delta G^{\dagger}=\Delta H^{\dagger}-T\Delta S^{\dagger}$, $\Delta H^{\dagger}$, and $\Delta S^{\dagger}$ are the activation parameters for the $(PL)_2\rightarrow(PL)_1$ transition; and k_B, h, and R are the Boltzmann, Planck, and universal gas constants, respectively. Thus, the general equilibrium three-state exchange processes is completely described by four equilibrium and six activation parameters: ΔH_1, ΔS_1, ΔH_2, ΔS_2, $\Delta H_1^{\dagger}$, $\Delta S_1^{\dagger}$, $\Delta H_2^{\dagger}$, $\Delta S_2^{\dagger}$, $\Delta H^{\dagger}$, and $\Delta S^{\dagger}$. The populations can be readily calculated from these parameters using the conditions for detailed balance (microscopic reversibility), $p_kk_{kl}=p_lk_{lk}$ and the fact that $\sum_k p_k=1$. The consecutive $P+L\leftrightarrow(PL)_1\leftrightarrow(PL)_2$ and parallel $(PL)_1\leftrightarrow P+L\leftrightarrow(PL)_2$ binding models are limiting cases of the general triangular model. The former is obtained by setting $k_{B_2F}=k_{FB_2}=0$ in Eq. (11), while the latter model is generated with $k_{B_2B_1}=k_{B_1B_2}=0$. Thus, there are eight thermodynamic/activation parameters that are necessary to fully describe each of the models that reduce to six in the limit of fast interconversion between $(PL)_1$ and P, as is the case here. Note that fast exchange can be modeled by (arbitrarily) setting k_{off1} to a very high value (e.g., 10^6/s).

The above discussion establishes that for the specific cases considered here, the three-state binding models include $n_tn_fn_r+2n_r+6$ parameters: $n_tn_fn_r$ intrinsic R_2 relaxation rates (assumed to be the same for all states), $2n_r$ temperature-independent chemical shift differences, $\Delta\varpi_{B_1F}=\varpi_{B_1}-\varpi_F$ and $\Delta\varpi_{B_2F}=\varpi_{B_2}-\varpi_F$, along with the six thermodynamic/activation parameters mentioned above.

Because the temperature-dependent ^{15}N CPMG data are well fit to a two-state binding model, including $n_tn_fn_r+n_r+4$ adjustable parameters, the extraction of $n_tn_fn_r+2n_r+6$ parameters based on the three-state models above requires an additional n_r+2 parameters that must be independently determined by other methods. These additional parameters are the n_r chemical shift differences, $\Delta\varpi_{titr}$, and $K_{d,titr}$, obtained from NMR titration data and the calorimetric association enthalpy, ΔH_{cal} [for the process $P+L\leftrightarrow\{(PL)_1,(PL)_2\}$], measured by ITC (see below for more details). Note that we have neglected any potential temperature dependence in the thermodynamic and activation parameters. In this regard, the relatively small temperature range over which data were collected (18 °C) is noteworthy. The parameters of the $P+L\leftrightarrow(PL)_1\leftrightarrow(PL)_2$ and $(PL)_1\leftrightarrow P+L\leftrightarrow(PL)_2$ binding models (they are equivalent) can therefore be extracted by a global three-state fit of ^{15}N CPMG relaxation dispersion data for n_r selected residues measured at all temperatures and magnetic fields while enforcing Eqs. (1), (2), and (4) (n_r+2 relationships; see Results and Discussion). Specifically, values of $K_{d,titr}$ and $dK_{d,titr}/dT$ [Eqs. (1) and (2)] at 25 °C were fixed to 200 μM and −0.7 μM/K (as obtained from NMR titration and ITC data), respectively, while the relations that connect $\Delta\varpi_{B_1F}$ and $\Delta\varpi_{B_2F}$ with $\Delta\varpi_{titr}$ were enforced [Eq. (4)]. Note that relaxation dispersion data do not provide information about the signs of $\Delta\varpi_{B_1F}$ and $\Delta\varpi_{B_2F}$ [although the relative signs of $\Delta\varpi_{B_1F}$ and $\Delta\varpi_{B_2F}$ can be determined; see Eq. (4)], since the data are equally well fit using either $\Delta\varpi_{disp}$ or $-\Delta\varpi_{disp}$. Here, we assumed that $\Delta\varpi_{disp}$ and $\Delta\varpi_{titr}$ have the same sign, since the opposite assumption produced unreasonable $\Delta\varpi_{B_1F}$ and $\Delta\varpi_{B_2F}$ values that were comparable in magnitude but opposite in sign for each residue.

Errors of the three-state binding parameters were estimated using a jackknife procedure[34] where data for 30% of the NH groups (nine and four residues for ubiquitin and SH3-C, respectively) were randomly removed and the data were subsequently refit (process repeated 10 times). With the use of the n_r+2 constraints described above, both three-state and two-state models have the same numbers of degrees of freedom and (as expected) result in the same quality of data fit (i.e., the same values of the global χ^2 target function).

In order to gain insight into *why* the $n_tn_fn_r+2n_r+6$ parameters of each of the three-state binding models [$P+L\leftrightarrow(PL)_1\leftrightarrow(PL)_2$ and $(PL)_1\leftrightarrow P+L\leftrightarrow(PL)_2$] can be obtained from the analysis considered above, it is useful to consider an alternate solution of the problem in which the $n_tn_fn_r+2n_r+6$ parameters of the three-state models are calculated directly from the apparent two-state parameters obtained from (i) two-state fits of ^{15}N CPMG relaxation dispersion data (that include $n_tn_fn_r+n_r+4$ parameters), (ii) two-state fits of NMR titration profiles (n_r+1 parameters), and (iii) ITC data (1 parameter). This is accomplished by solving a system of equations that relate the three-state parameters and apparent two-state parameters. An important relation in what follows is Eq. (1) in Results and Discussion, which can be directly obtained from Eq. (7) (as an aid to the reader, we repeat it here along with other equations that are relevant):

$$K_{d,titr}^{-1} = K_{d1}^{-1} + K_{d2}^{-2}, \tag{13}$$

where K_{d1} and K_{d2} are dissociation constants for $(PL)_1$ and $(PL)_2$, respectively. An additional useful relation can be obtained by noting that the relaxation dispersion profiles are well fit by an apparent two-state model in which P and $(PL)_1$ are in fast exchange such that the apparent K_d that is obtained from analysis of these data is given by

$$K_{d,disp} = \frac{\left([P] + [(PL)_1]\right)[L]_{disp}}{[(PL)_2]} = \frac{1 + K_{d1}^{-1}[L]}{K_{d2}^{-1}[L]}[L]_{disp} \tag{14}$$

Equation (14) can be rearranged to give

$$\frac{K_{d2}^{-1}[L]}{1+K_{d1}^{-1}[L]} = K_{d,disp}^{-1}[L]_{disp} \quad (15)$$

In Eqs. (14) and (15), [L] (concentration of free ligand from the three-state binding model) is calculated from Eq. (6) by substituting $K_{d,titr}$ for K_d, while $[L]_{disp}$ the free ligand concentration obtained from fitting the relaxation dispersion data to a two-state binding model, $\{P,(PL)_1\} \leftrightarrow (PL)_2$, is calculated directly from Eq. (6) by substituting $K_{d,disp}$ for K_d. Note that, in general, $[L] \neq [L]_{disp}$, since $[L] = L_0 - [(PL)_1] - [(PL)_2]$, while $[L]_{disp} = L_0 - [(PL)_2]$. Equations (13) and (15) can be recast in a way that connects the equilibrium three-state thermodynamic parameters ΔH_1, ΔS_1, ΔH_2, and ΔS_2 with the apparent two-state ΔH and ΔS obtained from two-state fits of the relaxation dispersion data, ΔH_{cal}, measured by ITC, and $K_{d,titr} = \exp(\Delta G_{titr}/(RT))$, derived from titration profiles

$$\exp(-(\Delta H_1 - T\Delta S_1)/(RT)) + \exp(-(\Delta H_2 - T\Delta S_2)/(RT)) = \exp(-\Delta G_{titr}/(RT)) \quad (16)$$

$$\exp(-(\Delta H_2 - T\Delta S_2)/(RT))[L] / (\exp(-(\Delta H_1 - T\Delta S_1)/(RT))[L] + 1) = \exp(-(\Delta H - T\Delta S)/(RT))[L]_{disp} \quad (17)$$

where $K_{d,disp} = \exp((\Delta H - T\Delta S)/(RT))$ and $K_{di} = \exp((\Delta H_i - T\Delta S_i)/(RT))$ ($i = 1,2$). Equations (16) and (17) follow directly from Eqs. (13) and (15), respectively. Note that all thermodynamic values ΔX are defined in terms of the ligand-binding reactions $P + L \leftrightarrow (PL)_1$ and $P + L \leftrightarrow (PL)_2$ (i.e., $X_{bound} - X_{free}$).

Two additional relationships can be obtained by equating the temperature derivatives of the right and left sides of Eqs. (16) and (17) to produce Eqs. (18) and (19), respectively:

$$\begin{aligned} &d/dT\left(\exp(-(\Delta H_1 - T\Delta S_1)/(RT)) + \exp(-(\Delta H_2 - T\Delta S_2)/(RT))\right) \\ &= d/dT\left(\exp(-(\Delta H_{cal} - T\Delta S^*)/(RT))\right) \end{aligned} \quad (18)$$

$$\begin{aligned} &d/dT\left(\exp(-(\Delta H_2 - T\Delta S_2)/(RT))[L] / (\exp(-(\Delta H_1 - T\Delta S_1)/(RT))[L] + 1)\right) \\ &= d/dT(\exp(-(\Delta H - T\Delta S)/(RT))[L]_{disp}), \end{aligned} \quad (19)$$

where ΔS^* is calculated from the known values of ΔH_{cal} and ΔG_{titr} that have been measured at 25 °C ($\Delta G_{titr} = \Delta H_{cal} - T\Delta S^*$). In Eqs. (18) and (19), we assume that ΔH and ΔS are temperature independent (ΔC_p of binding is 0) but note that the values of [L] and $[L]_{disp}$ are not since they depend on K_{di} ($K_{d,titr}$) and $K_{d,disp}$ [Eq. (6)], respectively; the temperature dependencies of [L] and $[L]_{disp}$ must therefore be taken into account in Eqs. (18) and (19). Thus, by solving the system of four equations, Eqs. (16)–(19), in terms of the four unknowns, ΔH_1, ΔS_1, ΔH_2, and ΔS_2, the equilibrium thermodynamic parameters of the three-state binding models, $P + L \leftrightarrow (PL)_1 \leftrightarrow (PL)_2$ and $(PL)_1 \leftrightarrow P + L \leftrightarrow (PL)_2$, can be obtained from parameters derived from relaxation dispersion, titration, and ITC data that are based on the simple two-state binding model. Note that Eqs. (16)–(19) are valid for both three-state models such that identical equilibrium entropy/enthalpy differences are obtained in both cases.

In addition to the equilibrium thermodynamic parameters that are obtained in fits of the dispersion data, values of activation enthalpy and entropy are also generated. These correspond to the activation parameters for the $(PL)_2 \rightarrow (PL)_1$ transition in the $P + L \leftrightarrow (PL)_1 \leftrightarrow (PL)_2$ model and for the $(PL)_2 \rightarrow P + L$ transition in the case of the $(PL)_1 \leftrightarrow P + L \leftrightarrow (PL)_2$ model, from which $k_{B_2B_1}$ and k_{B_2F} are calculated, respectively. Note that $k_{B_2B_1}$ (consecutive model) is therefore the same as k_{B_2F} (parallel model), although the corresponding values $k_{B_1B_2}$ and k_{FB_2} are not; these are obtained from detailed balance,

$$k_{B_1B_2} = \frac{p_{B_2}}{p_{B_1}} k_{B_2B_1}, \quad k_{FB_2} = \frac{p_{B_2}}{p_F} k_{B_2F}, \quad p_F = \frac{1}{1 + K_{d,titr}^{-1}[L]},$$
$$p_{Bi} = \frac{K_{di}^{-1}[L]}{1 + K_{d,titr}^{-1}[L]} \quad (i = 1,2), \quad (20)$$

where p_F, p_{B_1} and p_{B_2} are equilibrium populations of states F, B_1, and B_2, respectively. Based on the above discussion, it is not surprising that the energy profiles for the consecutive and parallel models (Fig. 3c and d and Fig. 4) are essentially the same. The only differences [aside from the rearrangement of P, $(PL)_1$, and $(PL)_2$ in the figures that reflects the difference in connectivities in the two models] are the value of one of the barriers and the identity of the states that are on either side of this barrier [$(PL)_1$ and $(PL)_2$ for the consecutive model and P and $(PL)_2$ for the parallel model].

The chemical shift differences $\Delta\varpi_{B_1F} = \varpi_{B_1} - \varpi_F$ and $\Delta\varpi_{B_2F} = \varpi_{B_2} - \varpi_F$ that pertain to the three-state binding models $P + L \leftrightarrow (PL)_1 \leftrightarrow (PL)_2$ and $(PL)_1 \leftrightarrow P + L \leftrightarrow (PL)_2$ can be directly calculated from the apparent two-state shift differences $\Delta\varpi_{disp}$ and $\Delta\varpi_{titr}$ obtained from relaxation dispersion and titration data, respectively, by solving Eqs. (3) and (4) (see Results and Discussion):

$$\Delta\varpi_{B_1F} = (\Delta\varpi_{titr}(p_{B_1} + p_{B_2}) - \Delta\varpi_{disp}p_{B_2})(p_F + p_{B_1})/p_{B_1} \quad (21)$$

$$\Delta\varpi_{B_2F} = \Delta\varpi_{titr}(p_{B_1} + p_{B_2}) + \Delta\varpi_{disp}(p_F + p_{B_1}), \quad (22)$$

where p_F, p_{B_1}, and p_{B_2} are calculated from the three-state thermodynamic parameters at 25 °C. As described above, in these calculations, it is always assumed that $\Delta\varpi_{disp}$ (or $\Delta\varpi_{B_2F}$) and $\Delta\varpi_{titr}$ have the same sign. Note that identical chemical shift differences are obtained for both three-state binding models.

Acknowledgements

This work was supported by a grant from the Canadian Institutes of Health Research to L.E.K. L.E.K. holds a Canada Research Chair in Biochemistry.

References

1. Fersht, A. (1999). *Structure and Mechanism in Protein Science: A Guide to Enzyme Catalysis and Protein Folding*. W. H. Freeman, New York, NY.
2. Schuck, P. W. (2007). *Protein Interactions: Biophysical Approaches for the Study of Complex Reversible Systems.* Springer, New York, NY.

3. Lo Conte, L., Chothia, C. & Janin, J. (1999). The atomic structure of protein–protein recognition sites. *J. Mol. Biol.* **285**, 2177–2198.
4. Jelesarov, I. & Bosshard, H. R. (1999). Isothermal titration calorimetry and differential scanning calorimetry as complementary tools to investigate the energetics of biomolecular recognition. *J. Mol. Recognit.* **12**, 3–18.
5. Schreiber, G. (2002). Kinetic studies of protein–protein interactions. *Curr. Opin. Struct. Biol.* **12**, 41–47.
6. Kay, L. E. (2005). NMR studies of protein structure and dynamics. *J. Magn. Reson.* **173**, 193–207.
7. Palmer, A. G., Kroenke, C. D. & Loria, J. P. (2001). Nuclear magnetic resonance methods for quantifying microsecond-to-millisecond motions in biological macromolecules. *Methods Enzymol.* **339**, 204–238.
8. Kern, D., Eisenmesser, E. Z. & Wolf-Watz, M. (2005). Enzyme dynamics during catalysis measured by NMR spectroscopy. *Methods Enzymol.* **394**, 507–524.
9. Ishima, R. & Torchia, D. A. (2000). Protein dynamics from NMR. *Nat. Struct. Biol.* **7**, 740–743.
10. Montelione, G. T. & Wagner, G. (1989). 2D chemical exchange NMR spectroscopy by proton-detected heteronuclear correlation. *J. Am. Chem. Soc.* **111**, 3096–3098.
11. Takeuchi, K. & Wagner, G. (2006). NMR studies of protein interactions. *Curr. Opin. Struct. Biol.* **16**, 109–117.
12. Zuiderweg, E. R. P. (2002). Mapping protein–protein interactions in solution by NMR spectroscopy. *Biochemistry*, **41**, 1–7.
13. Shuker, S. B., Hajduk, P. J., Meadows, R. P. & Fesik, S. W. (1996). Discovering high-affinity ligands for proteins: SAR by NMR. *Science*, **274**, 1531–1534.
14. Kern, D. & Zuiderweg, E. R. P. (2003). The role of dynamics in allosteric regulation. *Curr. Opin. Struct. Biol.* **13**, 748–757.
15. Matsuo, H., Walters, K. J., Teruya, K., Tanaka, T., Gassner, G. T., Lippard, S. J. *et al.* (1999). Identification by NMR spectroscopy of residues at contact surfaces in large, slowly exchanging macromolecular complexes. *J. Am. Chem. Soc.* **121**, 9903–9904.
16. Korchuganov, D. S., Nolde, S. B., Reibarkh, M. Y., Orekhov, V. Y., Schulga, A. A., Ermolyuk, Y. S. *et al.* (2001). NMR study of monomer–dimer equilibrium of barstar in solution. *J. Am. Chem. Soc.* **123**, 2068–2069.
17. Mittag, T., Schaffhausen, B. & Gunther, U. L. (2004). Tracing kinetic intermediates during ligand binding. *J. Am. Chem. Soc.* **126**, 9017–9023.
18. Haglund, K., Shimokawa, N., Szymkiewicz, I. & Dikic, I. (2002). Cbl-directed monoubiquitination of CIN85 is involved in regulation of ligand-induced degradation of EGF receptors. *Proc. Natl Acad. Sci. USA*, **99**, 12191–12196.
19. Soubeyran, P., Kowanetz, K., Szymkiewicz, I., Langdon, W. Y. & Dikic, I. (2002). Cbl-CIN85–endophilin complex mediates ligand-induced downregulation of EGF receptors. *Nature*, **416**, 183–187.
20. Bezsonova, I., Bruce, M. C., Wiesner, S., Lin, H., Rotin, D. & Forman-Kay, J. D. (2008). Interactions between the three CIN85 SH3 domains and ubiquitin: implications for CIN85 ubiquitination. *Biochemistry*, **47**, 8937–8949.
21. Hicke, L., Schubert, H. L. & Hill, C. P. (2005). Ubiquitin-binding domains. *Nat. Rev. Mol. Cell Biol.* **6**, 610–621.
22. Korzhnev, D. M., Salvatella, X., Vendruscolo, M., Di Nardo, A. A., Davidson, A. R., Dobson, C. M. & Kay, L. E. (2004). Low-populated folding intermediates of Fyn SH3 characterized by relaxation dispersion NMR. *Nature*, **430**, 586–590.
23. Grey, M. J., Tang, Y. F., Alexov, E., McKnight, C. J., Raleigh, D. P. & Palmer, A. G. (2006). Characterizing a partially folded intermediate of the villin headpiece domain under non-denaturing conditions: contribution of His41 to the pH-dependent stability of the N-terminal subdomain. *J. Mol. Biol.* **355**, 1078–1094.
24. Sugase, K., Dyson, H. J. & Wright, P. E. (2007). Mechanism of coupled folding and binding of an intrinsically disordered protein. *Nature*, **447**, 1021–1025.
25. Sugase, K., Lansing, J. C., Dyson, H. J. & Wright, P. E. (2007). Tailoring relaxation dispersion experiments for fast-associating protein complexes. *J. Am. Chem. Soc.* **129**, 13406–13407.
26. Tolkatchev, D., Xu, P. & Ni, F. (2003). Probing the kinetic landscape of transient peptide–protein interactions by use of peptide ^{15}N NMR relaxation dispersion spectroscopy: binding of an antithrombin peptide to human prothrombin. *J. Am. Chem. Soc.* **125**, 12432–12442.
27. Carr, H. Y. & Purcell, E. M. (1954). Effects of diffusion on free precession in nuclear magnetic resonance experiments. *Phys. Rev.* **94**, 630–638.
28. Meiboom, S. & Gill, D. (1958). Modified spin–echo method for measuring nuclear relaxation times. *Rev. Sci. Instrum.* **29**, 688–691.
29. Carver, J. P. & Richards, R. E. (1972). General two-site solution for the chemical exchange produced dependence of T_2 upon the Carr–Purcell pulse separation. *J. Magn. Reson.* **6**, 89–105.
30. Eyring, H. (1935). The activated complex in chemical reactions. *J. Chem. Phys.* **3**, 107–115.
31. Davis, D. G., Perlman, M. E. & London, R. E. (1994). Direct measurements of the dissociation rate constant for inhibitor–enzyme complexes via the $T_1\rho$ and T_2 CPMG methods. *J. Magn. Reson., Ser. B*, **104**, 266–275.
32. Ross, P. D. & Subramanian, S. (1981). Thermodynamics of protein association reactions—forces contributing to stability. *Biochemistry*, **20**, 3096–3102.
33. Alsallaq, R. & Zhou, H. X. (2008). Electrostatic rate enhancement and transient complex of protein–protein association. *Proteins*, **71**, 320–335.
34. Press, W. H., Teukolsky, S. A., Vetterling, W. T. & Flannery, B. P. (1997). *Numerical Recipes in C: The Art of Scientific Computing*, 2nd edit. Cambridge University Press, Cambridge, UK.
35. Wishart, D. S. & Case, D. A. (2001). Use of chemical shifts in macromolecular structure determination. *Methods Enzymol.* **338**, *3–34.*
36. Pawson, T. & Nash, P. (2003). Assembly of cell regulatory systems through protein interaction domains. *Science*, **300**, 445–452.
37. Pawson, T. (1995). Protein modules and signaling networks. *Nature*, **373**, 573–580.
38. Tollinger, M., Skrynnikov, N. R., Mulder, F. A. A., Forman-Kay, J. D. & Kay, L. E. (2001). Slow dynamics in folded and unfolded states of an SH3 domain. *J. Am. Chem. Soc.* **123**, 11341–11352.
39. Millet, O., Loria, J. P., Kroenke, C. D., Pons, M. & Palmer, A. G. (2000). The static magnetic field dependence of chemical exchange line-broadening defines the NMR chemical shift time scale. *J. Am. Chem. Soc.* **122**, 2867–2877.
40. McConnell, H. M. (1958). Reaction rates by nuclear magnetic resonance. *J. Chem. Phys.* **28**, 430–431.